Science Advances
AAAS

Supplementary Materials for

Direct detection of human adenovirus or SARS-CoV-2 with ability to inform infectivity using DNA aptamer-nanopore sensors

Ana S. Peinetti, Ryan J. Lake, Wen Cong, Laura Cooper, Yuting Wu, Yuan Ma, Gregory T. Pawel, María Eugenia Toimil-Molares*, Christina Trautmann, Lijun Rong*, Benito Mariñas*, Omar Azzaroni*, Yi Lu*

*Corresponding author. Email: yi-lu@illinois.edu (Y.L.); azzaroni@inifta.unlp.edu.ar (O.A.); marinas@illinois.edu (B.M.); lijun@uic.edu (L.R.); m.e.toimilmolares@gsi.de (M.E.T.-M.)

Published 22 September 2021, *Sci. Adv.* **7**, eabh2848 (2021)
DOI: 10.1126/sciadv.abh2848

The PDF file includes:

Supplementary Text

Supplementary Text 1. A comparison between plaque assays, qPCR, and our aptamer-nanopore sensor.

We have quantified the infectious HAdV concentration using plaque assays and benchmarked our results with this, as it is still considered the gold standard method to quantify infectious virus, since simpler and more recently developed methods like qPCR and immunoassays are not capable of distinguishing noninfectious/inactivated virus from active virus (*11*). It is likely that the efficiency of infectivity determined by plaque assay is lower than 100% because some infective viruses that reach the surface of host cells in the plaque assay might not locate protein receptors involved in the initial attachment steps of the infection cycle, ultimately resulting in the formation of plaques. Although to date there is no method to determine what portion of the overall concentration of infective virions is obtained by plaque assay, a comparison could be made between results from plaque assays and qPCR measurements of genome copies in the same samples. In a previous study, members of our team quantified (in triplicate) HAdV-2 samples with both plaque assay and qPCR (*55*). The results reproduced in Table S1 reveal a ratio of ≈150 copies/pfu. Unfortunately, the number of genome copies could not be considered to directly correspond to infective viruses because some copies could be associated with incompletely assembled virions not capable of infection. An important point revealed by the stirring test data in Fig. S7 is that the regression has a stronger linear dependence compared to that of the tests without stirring. Extrapolation of the linear regression to $f_{rec}norm=1$ would result in an intercept of approximately 0.1 pfu/mL, suggesting that the sensor would have a sensitivity approximately one order of magnitude higher than that of the plaque assay. These results suggest that 1/15 genome copies could potentially correspond to infective viruses. Such a possibility is plausible because our aptamer method is targeting capsid proteins that are synthesized in the final steps of the infection cycle, and so the possibility that the signal corresponds to infective viruses is higher. If so, the concentration of infectious virions would be ten times that determined by plaque assay. In terms of our assay, this result indicates that, in the nanopore, we are not necessarily detecting a single infective particle in the sample, but the signal corresponds to an order of magnitude higher number, indicating that we reach the same or higher detection limit as the gold standard method, plaque assay, with a rapid and simple test. Moreover, this result highlights that plaque assays likely underestimate infectious virus concentration.

Table S1. Comparison between qPCR and plaque assay quantification of HAdV-2 samples. The number of DNA copies is measured by a 105-bp amplicon in the E1A gene.

Experiment	pfu/mL	DNA copies/mL	DNA copies/pfu
MC1	1.02×10^6	1.35×10^8	131
MC2	9.87×10^5	1.45×10^8	147
MC3	7.62×10^5	1.40×10^8	184
		Average:	154

Supplementary Text 2. Determination of detection and quantification limits.

Based on the linear regression obtained (Fig. S6a), it is possible to define the limit of detection as LoD= 3*σ/m, and the quantification limit as LoQ=10* σ/m, where m is the slope of the linear calibration (m = 0.123) and σ is the standard deviation of the intercept (σ = 0.0076). Then, to obtain the LoD and LoQ in pfu/mL units, we calculate the antilogarithm, because the linear regression is obtained from a logarithm scale in the x axis. Thus, the LoD = 1.5 pfu/mL and LoQ = 4 pfu/mL.

We have also compared, using a two-tailed Student's t test, the mean of the f_{rec}norm signal obtained for 1 pfu/mL of infectious HAdV with a) the mean f_{rec}norm value for different concentrations of infectious HAdV when no aptamer is grafted in the nanopore, and b) the mean f_{rec}norm for different concentrations of noninfectious HAdV after immobilization of the aptamer in the nanopore. We observed in both cases that these values are significantly different to the f_{rec}norm for 1 pfu/mL of infectious HAdV, with at least 99.9% and 99% confidence, respectively (Fig. S6). Thus, 1 pfu/mL of HAdV is indeed producing a signal distinguishable from these blanks.

Supplementary Text 3. Choice of Lentivirus Pseudotyped with SARS-CoV-2 S protein as the SELEX target.

It had previously been demonstrated that the S protein of SARS-CoV-1 was a good target for recognition, especially since it is the primary surface protein responsible for entry into cells, so the S protein of SARS-CoV-2 was deemed the most suitable target due to its similarity to SARS-CoV-1 (it interacts with the same ACE2 receptor for entry into cells). Other groups have already performed SELEX against the isolated S protein or RBD domain of the S protein of SARS-CoV-2 (*49-51*), as well as against the N protein (*56*). Because of our prior success in using whole virus SELEX to isolate the HAdV, we wanted to use a whole viral mimic of SARS-CoV-2 to better replicate the native state of the S protein. For instance, it is known that the S protein forms trimer structures when incorporated into the viral envelope, so using a solubilized S protein in its monomer form loses a significant amount of quaternary structure that could be used by aptamers for better recognition or may even inhibit binding of aptamers that have been selected against the solubilized protein. Other researchers have recently developed variations of the SARS-CoV-2 S protein that allow it to trimerize in its soluble form, but this target is still significantly different from the membrane bound S proteins found in the native system. Furthermore, the S protein in the pseudotyped virus is expressed as a glycoprotein with the same sugar modifications as in the SARS-CoV-2. Because of all these considerations, we desired to use a pseudotyped virus, in which a different virus is used as a backbone, which is incorporated with the SARS-CoV-2 S protein to mimic its native state within the viral envelope.

The Rong lab has extensive experience in creating lentivirus-based pseudoviruses, including for the SARS-CoV-1 S protein. Based on this expertise, we were able to create lentivirus pseudotyped with the SARS-CoV-2 S protein in a rapid manner, allowing us to use it as the target for our SELEX and for testing our nanopore sensor at BSL-2 levels while still maintaining high similarity to the S protein in its native viral envelope.

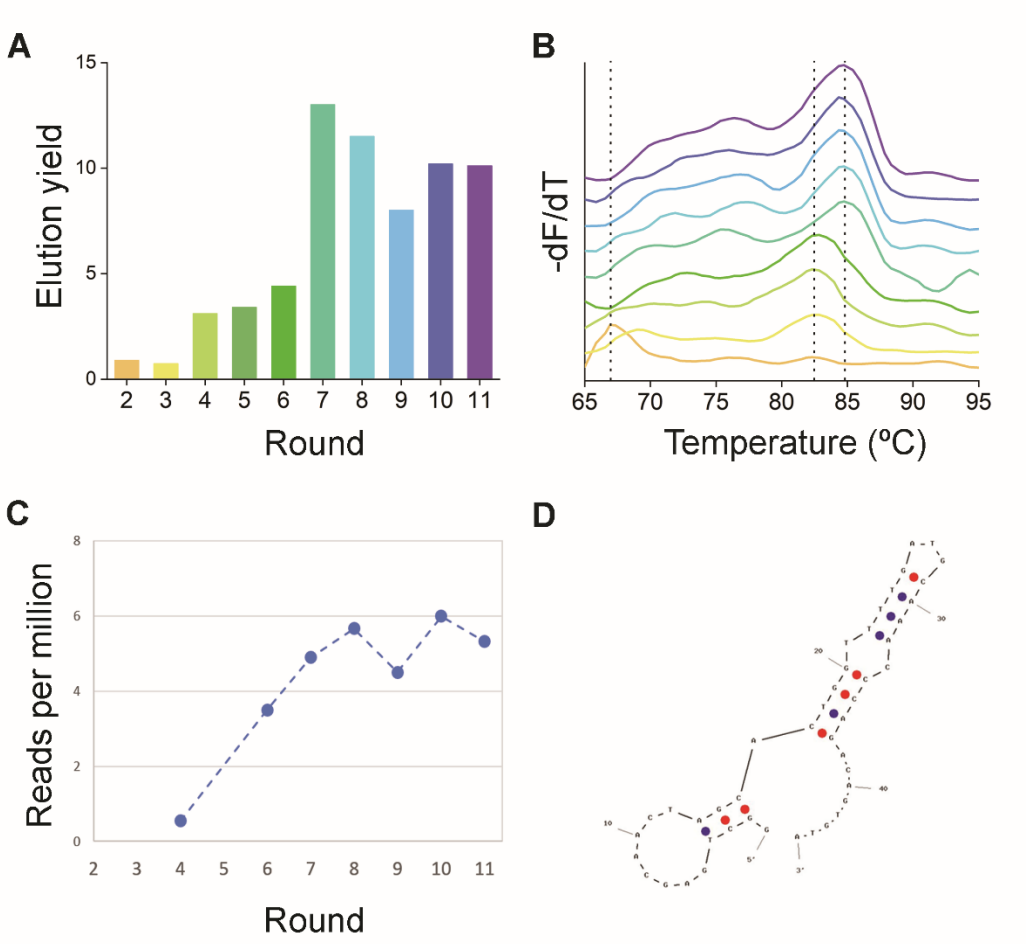

Fig. S1. ***In-vitro*** **selection of infectious HAdV-specific aptamers. (A)** Monitoring the progress of the SELEX process by quantification of the elution yield, i.e., bound ssDNA over total added ssDNA, using qPCR. **(B)** Melting curve for the different pools during HAdV aptamer selection. After round 3 (yellow), a peak at higher melting temperature (Tm) appeared and shifted from 82 ºC in the middle rounds to 85 ºC at round 7 (green), with its intensity increasing with subsequent rounds, suggesting that the DNA pool has converged from mostly random sequences with low Tm to more conserved sequences with higher Tm. **(C)** Reads per million (RPM) obtained from analysis of the HTS data for the HAdV-Seq4 sequence as a function of the selection rounds, using FASTAptamer-Count. **(D)** The predicted most stable secondary structure of the aptamer based on the UNAFold software. Calculations were made at 25 ºC, 100 mM NaCl and 2 mM $MgCl_2$.

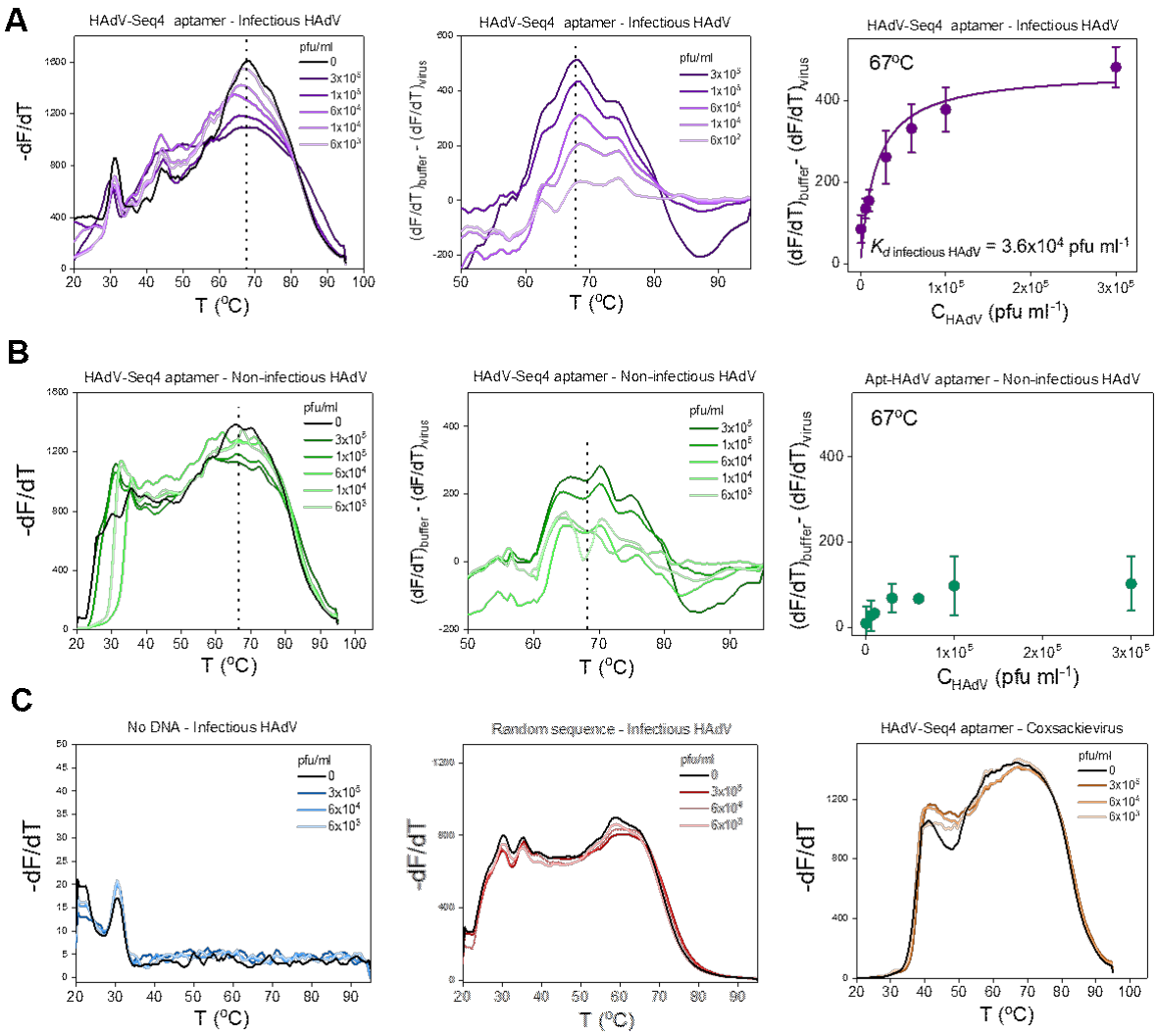

Fig. S2. **Thermofluorimetric analysis (TFA) of binding interaction of HAdV-Seq4 aptamer with HAdV using qPCR. (A)** From left to right, for infectious HAdV: TFA melt curves; difference of the melt curve between 0 pfu/mL virus and different concentrations of HAdV; and binding curve at 67 ºC in presence of 20 nM of HAdV-Seq4 aptamer based on triplicate data. We observed that the peak around 67 ºC changes with different concentrations of infectious HAdV, compared with the aptamer solution that does not contain the virus (just buffer, black line). Then, the change in the signal at 67 ºC was used to obtain the binding curve, by subtracting the signal without the virus, $(dF/dT)_{buffer}$, and the signal with different concentration of virus, $(dF/dT)_{virus}$. **(B)** Same as (A) but for non-infectious HAdV. In this case, no significant change is observed at 67 ºC or other temperature. **(C)** TFA melt curve for different negative controls: infectious HAdV without DNA, infectious HAdV with 20 nM of a random sequence with the same length of the HAdV-Seq4 aptamer, and coxsackievirus with 20 nM of HAdV-Seq4 aptamer.

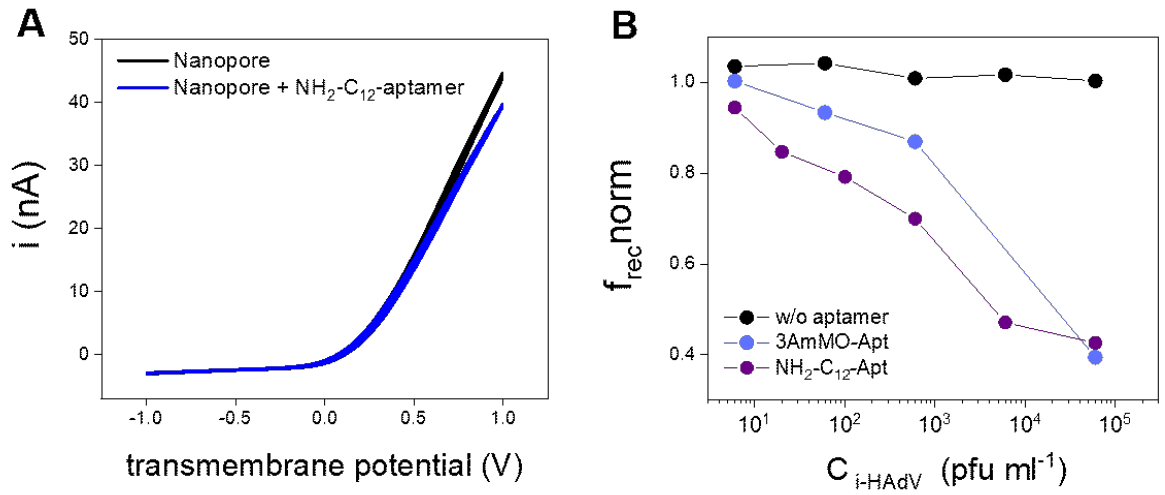

Fig. S3. **Modification of nanopore inner surface with HAdV aptamer. (A)** I-V curves of a nanopore system before (black) and after (blue) modification with NH_2-C_{12}-aptamer. **(B)** Normalized rectification efficiencies versus logarithm of the infectious HAdV concentration obtained for different amino modifications of the HAdV aptamer. To prevent the nanopore surface from interfering with the aptamer binding to its target, we added a spacer between the amine group and the aptamer. Also, the effect of different orientations of the HAdV aptamer on the surface was studied by introducing the amino modification on different ends of the sequence. Black corresponds to the nanopore without incorporation of the aptamer. Light blue corresponds to the nanopore modified with 3AmMO-aptamer (3' modification), and purple with NH_2-C_{12}-aptamer (5' modification). We found that the modification at 5' end with the longer spacer improved the sensitivity.

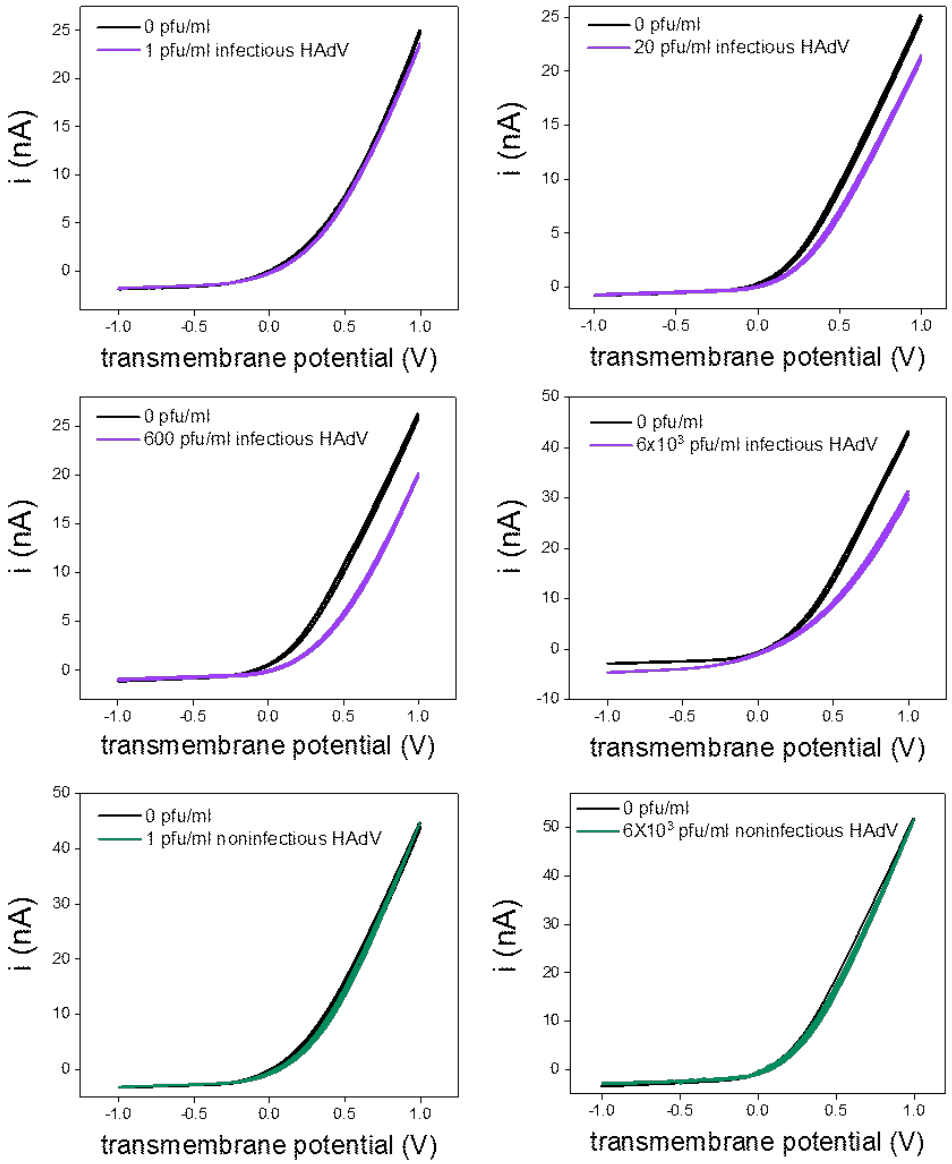

Fig. S4. **I-V curves for different nanopores modified with NH_2-C_{12}-aptamer**. Black corresponds to incubation of the aptamer-nanopore system with buffer (without virus, 0 pfu/mL) and, purple and green lines correspond to incubations with different concentrations of infectious HAdV or noninfectious HAdV, respectively. Comparing the differences in the I-V curves without virus and with virus for the same membrane, even for a high concentration (6×10^3 pfu/mL) of noninfectious HAdV, no changes were observed, while for 1 pfu/mL of infectious virus there is a decrease in the current at 1 V.

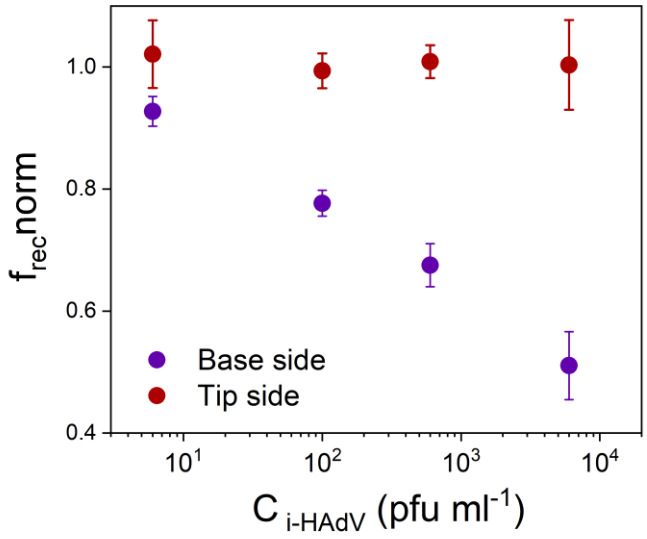

Fig. S5. **Effect of incubate the virus solution facing different sides of the asymmetrical nanopore on the aptamer-nanopore system performance.** Normalized rectification factor versus logarithm of the infectious HAdV concentration after 30 min incubation of the virus solution facing the base side of the nanopore (purple) and facing the tip side (red). No changes in the f_{rec}norm are observed when the virus sample is applied to the reservoir facing the narrow side (tip) of the nanopore. This indicates that the virus needs to be able to enter the nanopore to bind to the aptamer coating the inner surface of the nanopores. Due to the reduced tip size, this is possible only from the base. Tip diameter < 50 nm, base diameter: ≈900 nm.

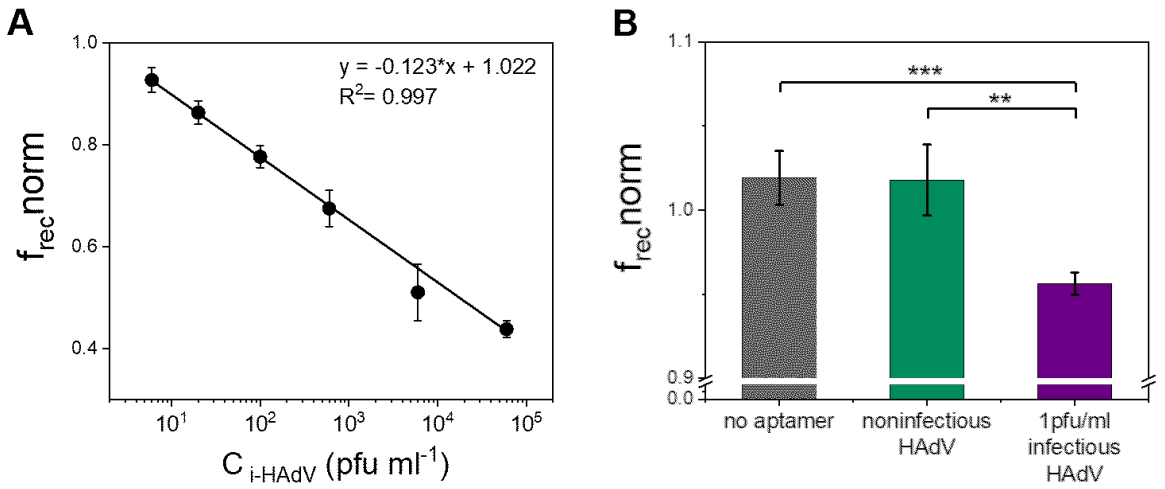

Fig. S6. **Sensitivity of the aptamer-nanopore system to detect HAdV. (A)** Linear dependence of normalized rectification efficiencies versus logarithm of infectious HAdV concentration with linear fitting. Each data point represents the mean and standard deviation of 3 replicates. **(B)** The aptamer-nanopore system can detect 1 pfu/mL of infectious HAdV. Normalized rectification efficiency of 1pfu/mL of infectious HAdV after aptamer immobilization on the nanopore (purple). Grey represents the mean and SD of f_{rec}norm for the different concentrations of infectious HAdV showed in Fig. 2b when no aptamer is grafted in the nanopore, while green represents the mean and SD of f_{rec}norm for the different concentrations of noninfectious HAdV showed in Fig. 2b after immobilization of the aptamer in the nanopore. two-tailed Student's t test; **p<0.01, ***p<0.001, bars represent mean ± SD.

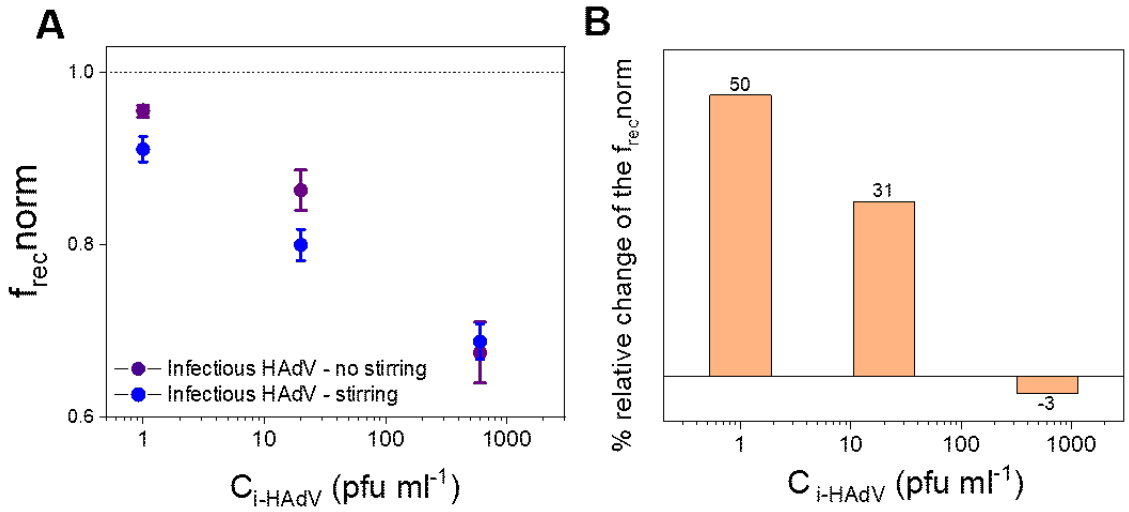

Fig. S7. Effect of stirring during virus incubation on the aptamer-nanopore system performance. (A) Normalized rectification factor versus logarithm of the infectious HAdV concentration after 30 min incubation of the virus solution with the aptamer-nanopore without stirring (purple) or with magnetic stirring (blue). **(B)** Relative change of the f_{rec}norm (defined as the percent change of 1-f_{rec}norm) when stirring is added compared with the relative f_{rec}norm without stirring, for different concentrations of infectious HAdV. The larger changes are observed for lower infectious HAdV concentrations, and at 600pfu/mL, no significant changes are observed.

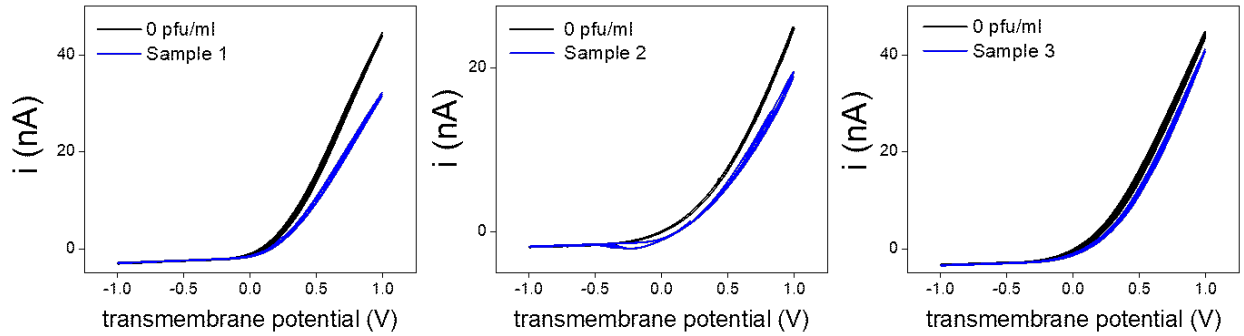

Fig. S8. **Detection of infectious HAdV in a buffer solution containing a mixture of infectious and non-infectious HAdV**. I-V curves for 3 samples prepared by treating an infectious HAdV sample ($7.2x10^3$ pfu/mL) with free chlorine and taking aliquots at different timepoints to obtain different degrees of inactivation with the same total amount of virus: 90% (sample 1), 99% (sample 2), and 99.9% (sample 3). The differences in the f_{rec} indicate that the aptamer-nanopore sensor can detect different infectious HAdV concentrations even when the total amount of virus is the same within different samples.

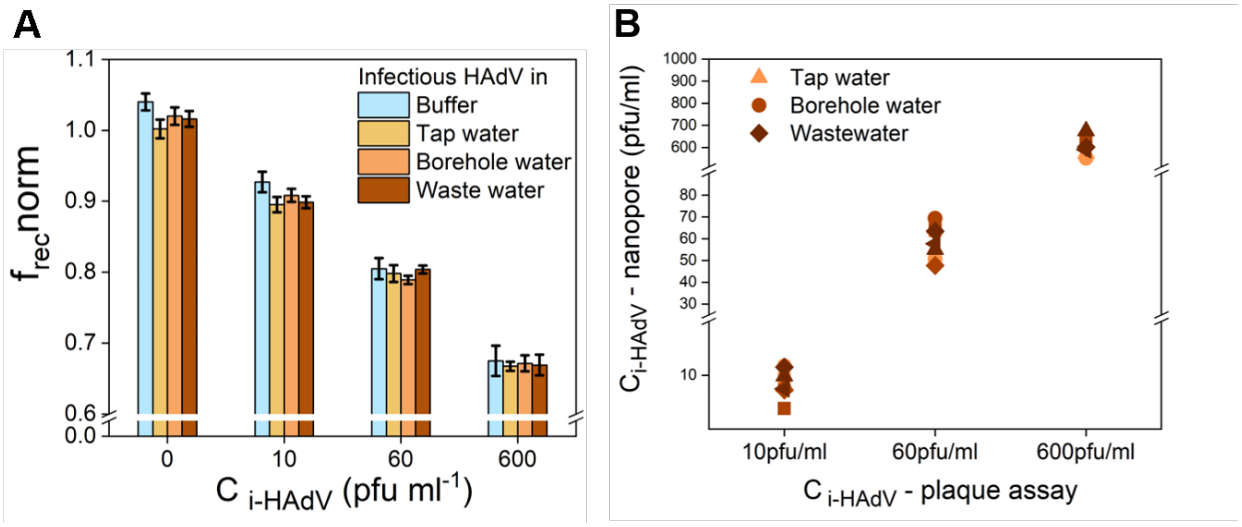

Fig. S9. **Detection of infectious HAdV in different real water samples. (A)** Normalized rectification efficiency obtained for different concentrations of infectious HAdV that were spiked in drinking water and wastewater. The f_{rec}norm measured for the same concentration of infectious virus in buffer (blue) was included for comparison. n=3, technical replicates (mean ± SD). **(B)** Individual values for each concentration (triplicate) for different environmental water samples.

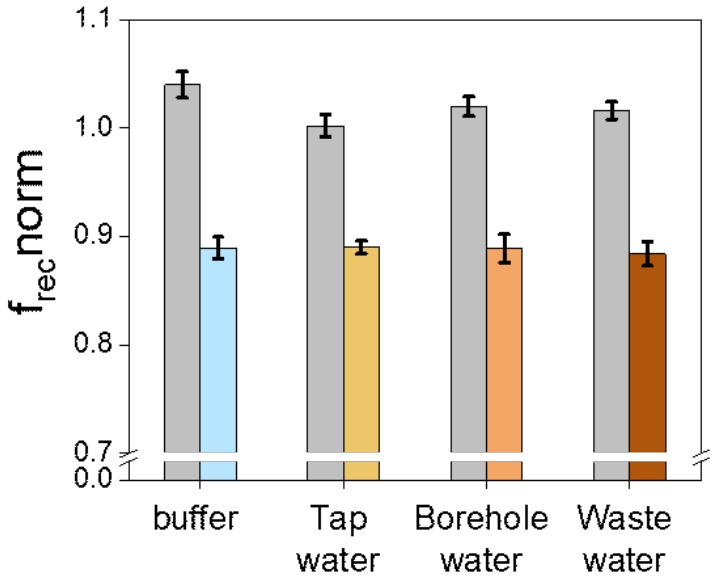

Fig. S10. **Detection of infectious HAdV in different real water samples containing a mixture of infectious and non-infectious HAdV.** Normalized rectification efficiency obtained for different water samples in presence of non HAdV (gray) and in a solution of HAdV with 99.9% inactivation (mixture of infectious and non-infectious viruses). n=3, technical replicates (mean ± SD).

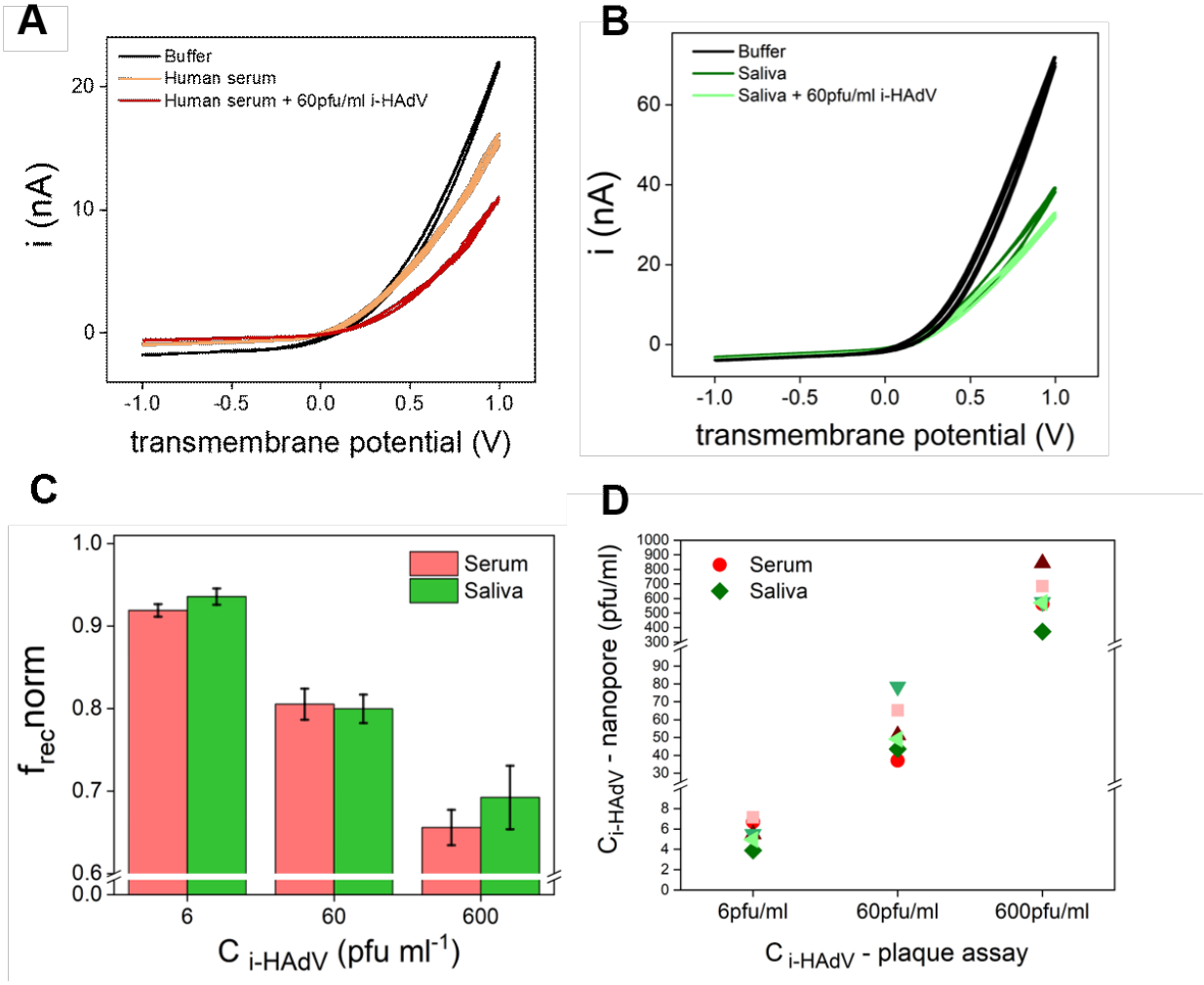

Fig. S11. **Detection of infectious HAdV in different biological samples. (A)** I-V curves for a human serum sample before (yellow) and after (red) being spiked with 60 pfu/mL infectious HAdV. There is a change in the I-V curve when the nanopore is incubated in human serum compared with the curve after incubation with buffer (black). To take these differences into account, the f_{rec} for the human serum samples with different concentrations of infectious HAdV were normalized by the measurement after incubation in human serum, instead of buffer. **(B)** I-V curves for a human saliva sample before (dark green) and after (light green) being spiked with 60 pfu/mL infectious HAdV. **(C)** Normalized rectification efficiency obtained for human serum and saliva samples spiked with different concentrations of infectious HAdV. n=3, technical replicates (mean ± SD). **(D)** Individual values for each concentration (triplicate) for different biological samples.

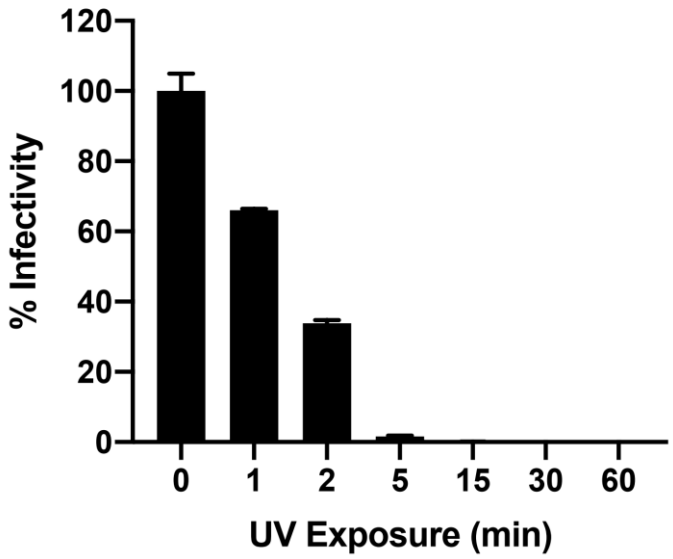

Fig. S12. **Monitoring the UV-light inactivation of SARS-CoV-2 pseudovirus at different exposure times by a luciferase assay.** In the case of pseudotyped particles, it is not possible to perform a plaque assay.

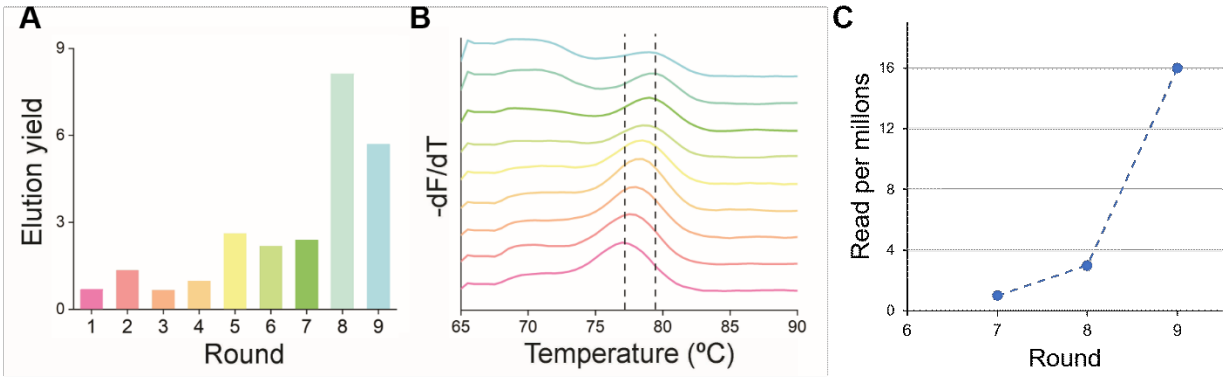

Fig. S13. ***In-vitro*** **selection of infectious SARS-CoV-2-specific aptamers. (A)** Monitoring the progress of SELEX process by quantification of the elution yield, i.e., the bound ssDNA over the added ssDNA, using qPCR. **(B)** Melting curve for the different pools during SARS-CoV-2 aptamer selection. The peak at high Tm shifted from 77ºC to 79ºC, suggesting that the DNA pool has converged from random sequences with low Tm to more conserved sequences with higher Tm. The colors correspond to the colors of the rounds in a. **(C)** Reads per millions (RPM) obtained by analysis of the HTS data for SARS2-AR10 sequence as a function of the selection rounds, using FASTAptamer-Count.

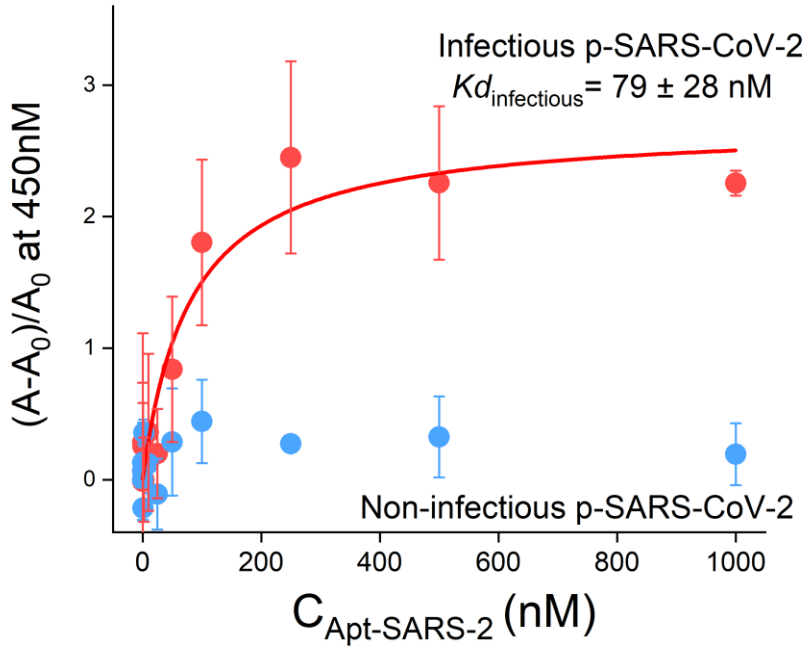

Fig. S14. **Binding curves of SARS2-AR10 aptamer and pseudotyped SARS-CoV-2 using ELONA assay.** $5x10^8$ copies/mL of pseudotyped SARS-CoV-2 are immobilized on a 96-well plate. The dissociation constant (K_d) of SARS2-AR10 sequence for the active pseudotyped SARS-CoV-2 is 79 nM, while no change in the absorbance at 450nm is observed for the inactive pseudotyped SARS-CoV-2. n = 3 technical replicates (mean ± SD).

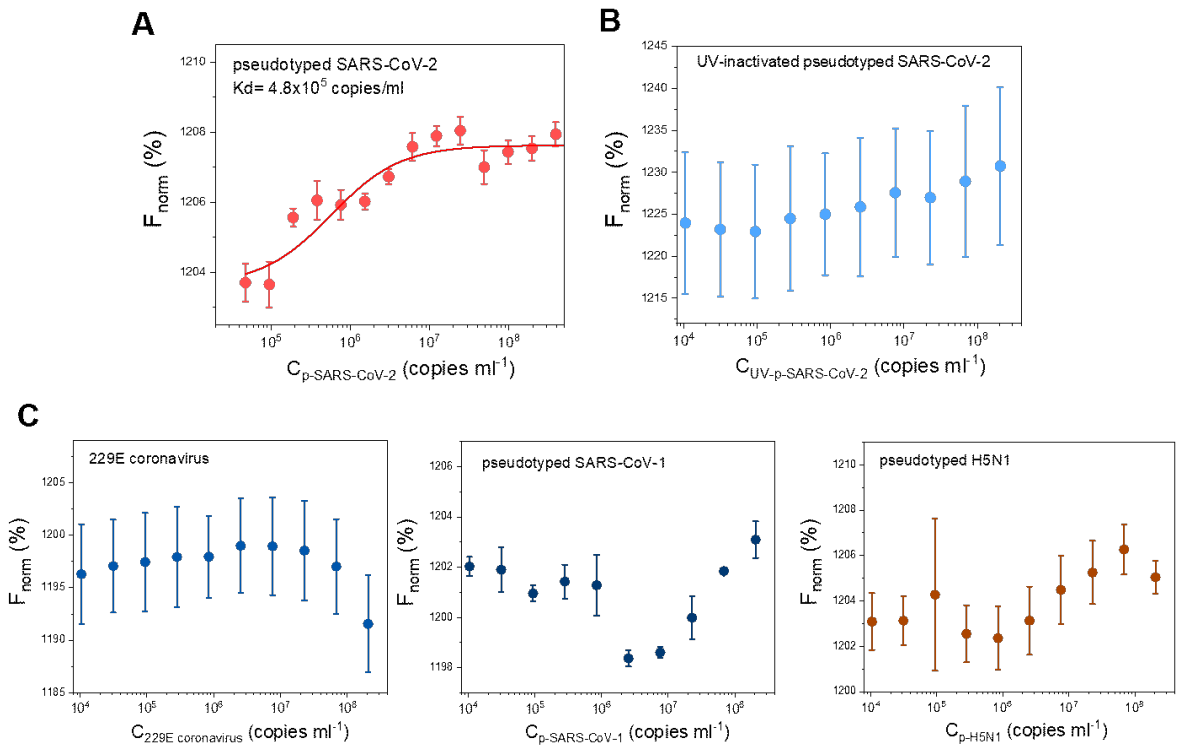

Fig. S15. **Binding curves of SARS2-AR10 aptamer and different viruses using MST technique.** MST results for: **(A)** active pseudotyped SARS-CoV-2, **(B)** UV-inactivated pseudotyped SARS-CoV-2 and **(C)** other viruses, including 229E coronavirus, pseudotyped SARS-CoV-1, and pseudotyped H5N1. SARS2-AR10 was labeled with FAM at the 5' end and its concentration was fixed at 250nM. These results confirm the binding of the aptamer to active pseudotyped SARS-CoV-2 and its selectivity. n = 3 technical replicates (mean ± SD).

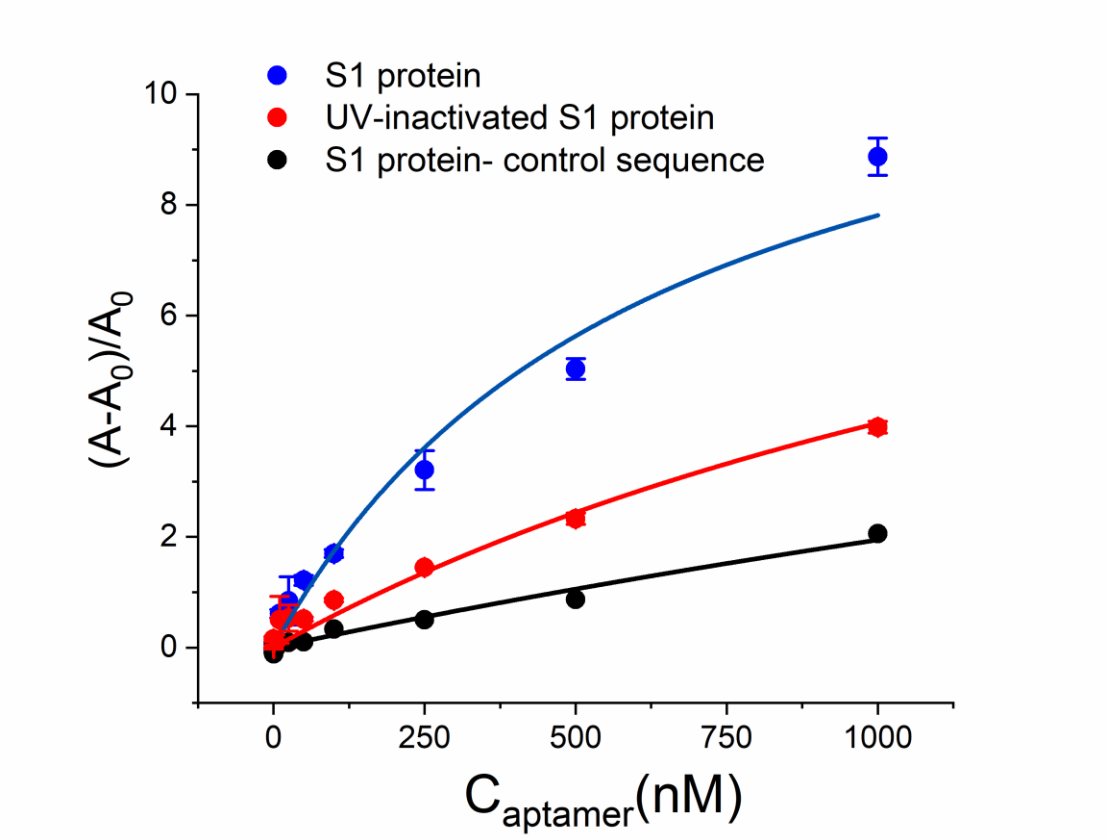

Fig. S16. Binding curves of SARS2-AR10 aptamer and SARS-CoV-2 S1 domain protein obtained by ELONA assay. Blue corresponds to active SARS-CoV-2 S1 domain protein and red to UV-inactivated SARS-CoV-2 S1 domain protein. The dissociation constant, K_d of the SARS2-AR10 aptamer for the active S1 protein is 630 nM, while the affinity to the UV-inactivated protein is lower (K_d = 2000nM). Black corresponds to the ELONA results for the binding of S1 protein to a control sequence. n = 3 technical replicates (mean ± SD).

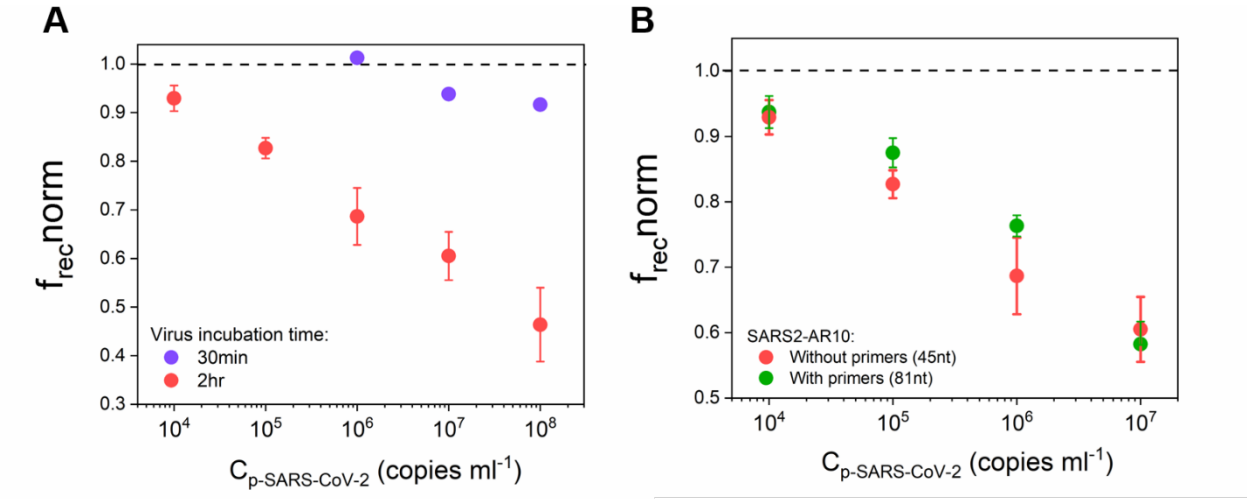

Fig. S17. **Effect of virus incubation time and length of the aptamer on the SARS2-AR10-nanopore system performance. (A)** Normalized rectification factor versus logarithm of the active pseudotyped SARS-CoV-2 concentration after 30min (purple) and 2hr (red) incubation time of the virus solution with the SARS2-AR10-nanopore system. **(B)** Comparison of the performance of the SARS2-AR10 with primers (81nt) and without primers (45nt). In both case the performance is comparable, thereby we choose the short version of the aptamer for further application in the nanopore.

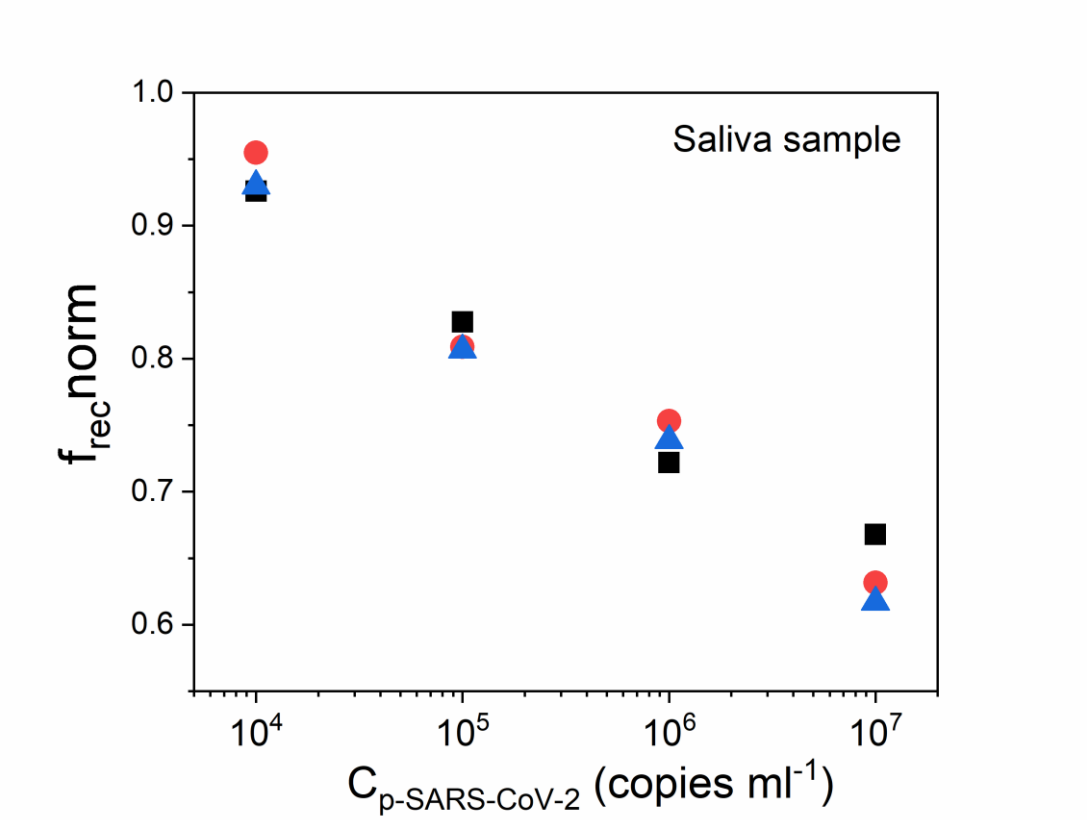

Fig. S18. **Detection of active pseudotyped SARS-CoV-2 in saliva samples.** Normalized rectification factor versus logarithm of the active pseudotyped SARS-CoV-2 concentration spiked in human saliva sample. A total of 12 saliva samples were spiked with different concentrations of infectious pseudotyped SARS-CoV-2 and each sample was measured with a different nanopore membrane.

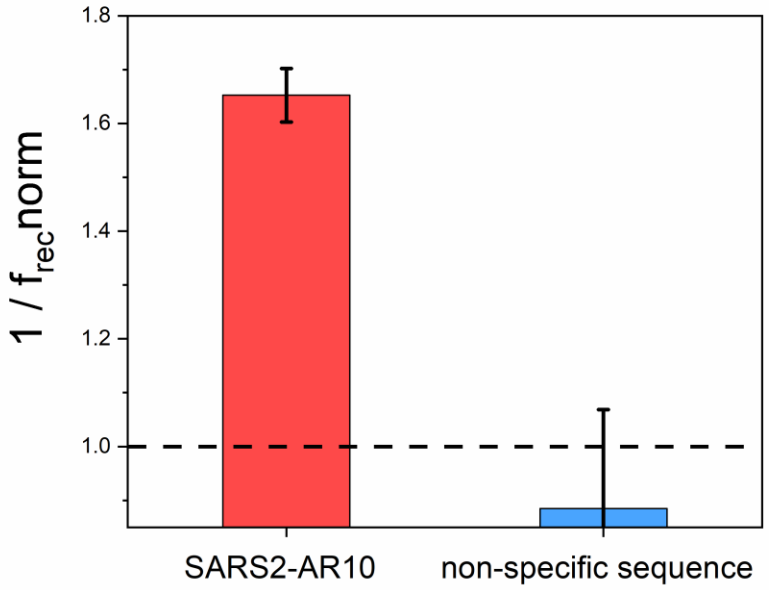

Fig. S19. Comparison of the aptamer-nanopore system signal using SARS2-AR10 aptamer vs using a control sequence. Inverse of the f_{rec}norm obtained for active pseudotyped SARS-CoV-2 (SARS-2) spiked in saliva using SARS2-AR10 aptamer in the nanopores (red) and a control sequence (blue). The concentration of the virus is $1x10^7$ copies/mL. n = 3 technical replicates (mean ± SD).

REFERENCES AND NOTES

1. D. Jacot, G. Greub, K. Jaton, O. Opota, Viral load of SARS-CoV-2 across patients and compared to other respiratory viruses. *Microbes Infect.* **22**, 617–621 (2020).

2. A. Ganguli, A. Mostafa, J. Berger, M. Y. Aydin, F. Sun, S. A. Stewart de Ramirez, E. Valera, B. T. Cunningham, W. P. King, R. Bashir, Rapid isothermal amplification and portable detection system for SARS-CoV-2. *Proc. Natl. Acad. Sci. U.S.A.* **117**, 22727–22735 (2020).

3. C. Myhrvold, C. A. Freije, J. S. Gootenberg, O. O. Abudayyeh, H. C. Metsky, A. F. Durbin, M. J. Kellner, A. L. Tan, L. M. Paul, L. A. Parham, K. F. Garcia, K. G. Barnes, B. Chak, A. Mondini, M. L. Nogueira, S. Isern, S. F. Michael, I. Lorenzana, N. L. Yozwiak, B. L. MacInnis, I. Bosch, L. Gehrke, F. Zhang, P. C. Sabeti, Field-deployable viral diagnostics using CRISPR-Cas13. *Science* **360**, 444–448 (2018).

4. I. Arevalo-Rodriguez, D. Buitrago-Garcia, D. Simancas-Racines, P. Zambrano-Achig, R. Del Campo, A. Ciapponi, O. Sued, L. Martinez-García, A. W. Rutjes, N. Low, P. M. Bossuyt, J. A. Perez-Molina, J. Zamora, False-negative results of initial RT-PCR assays for COVID-19: A systematic review. *PLOS ONE* **15**, e0242958 (2020).

5. F. Amanat, D. Stadlbauer, S. Strohmeier, T. H. O. Nguyen, V. Chromikova, M. McMahon, K. Jiang, G. A. Arunkumar, D. Jurczyszak, J. Polanco, M. Bermudez-Gonzalez, G. Kleiner, T. Aydillo, L. Miorin, D. S. Fierer, L. A. Lugo, E. M. Kojic, J. Stoever, S. T. H. Liu, C. Cunningham-Rundles, P. L. Felgner, T. Moran, A. García-Sastre, D. Caplivski, A. C. Cheng, K. Kedzierska, O. Vapalahti, J. M. Hepojoki, V. Simon, F. Krammer, A serological assay to detect SARS-CoV-2 seroconversion in humans. *Nat. Med.* **26**, 1033–1036 (2020).

6. C. Sheridan, Fast, portable tests come online to curb coronavirus pandemic. *Nat. Biotechnol.* **38**, 515–518 (2020).

7. R. Wölfel, V. M. Corman, W. Guggemos, M. Seilmaier, S. Zange, M. A. Müller, D. Niemeyer, T. C. Jones, P. Vollmar, C. Rothe, M. Hoelscher, T. Bleicker, S. Brünink, J. Schneider, R. Ehmann, K. Zwirglmaier, C. Drosten, C. Wendtner, Virological assessment of hospitalized patients with COVID-2019. *Nature* **581**, 465–469 (2020).

8. R. F. Service, Coronavirus antigen tests: Quick and cheap, but too often wrong? *Science* (2020).

9. R. Weissleder, H. Lee, J. Ko, M. J. Pittet, COVID-19 diagnostics in context. *Sci. Transl. Med.* **12**, eabc1931 (2020).

10. G. M. Joynt, W. K. Wu, Understanding COVID-19: What does viral RNA load really mean? *Lancet Infect. Dis.* **3099**, 19–20 (2020).

11. N. Cook, D. O. Cliver, Viruses: Detection, in *Encyclopedia of Food Microbiology* (Elsevier, 2014), vol. 3, pp. 727–731.

12. S. Khanal, P. Ghimire, A. Dhamoon, The repertoire of adenovirus in human disease: The innocuous to the deadly. *Biomedicine* **6**, 30 (2018).

13. M. R. Dunn, R. M. Jimenez, J. C. Chaput, Analysis of aptamer discovery and technology. *Nat. Rev. Chem.* **1**, 0076 (2017).

14. Z. Shen, Z. Wu, D. Chang, W. Zhang, K. Tram, C. Lee, P. Kim, B. J. Salena, Y. Li, A catalytic DNA activated by a specific strain of bacterial pathogen. *Angew. Chem. Int. Ed.* **55**, 2431–2434 (2016).

15. M. A. Page, J. L. Shisler, B. J. Mariñas, Kinetics of adenovirus type 2 inactivation with free chlorine. *Water Res.* **43**, 2916–2926 (2009).

16. K. Sefah, D. Shangguan, X. Xiong, M. B. O'Donoghue, W. Tan, Development of DNA aptamers using Cell-SELEX. *Nat. Protoc.* **5**, 1169–1185 (2010).

17. N. Kacherovsky, I. I. Cardle, E. L. Cheng, J. L. Yu, M. L. Baldwin, S. J. Salipante, M. C. Jensen, S. H. Pun, Traceless aptamer-mediated isolation of CD8+ T cells for chimeric antigen receptor T-cell therapy. *Nat. Biomed. Eng.* **3**, 783–795 (2019).

18. Q. Pan, F. Luo, M. Liu, X. L. Zhang, Oligonucleotide aptamers: Promising and powerful diagnostic and therapeutic tools for infectious diseases. *J. Infect.* **77**, 83–98 (2018).

19. C. L. A. Hamula, H. Peng, Z. Wang, G. J. Tyrrell, X.-F. Li, X. C. Le, An improved SELEX technique for selection of DNA aptamers binding to M-type 11 of Streptococcus pyogenes. *Methods* **97**, 51–57 (2016).

20. A. M. Gall, J. L. Shisler, B. J. Mariñas, Analysis of the viral replication cycle of adenovirus serotype 2 after inactivation by free chlorine. *Environ. Sci. Technol.* **49**, 4584–4590 (2015).

21. B. Vazquez-Bravo, K. Gonçalves, J. L. Shisler, B. J. Mariñas, Adenovirus replication cycle disruption from exposure to polychromatic ultraviolet irradiation. *Environ. Sci. Technol.* **52**, 3652–3659 (2018).

22. V. A. Avanzato, M. J. Matson, S. N. Seifert, R. Pryce, B. N. Williamson, S. L. Anzick, K. Barbian, S. D. Judson, E. R. Fischer, C. Martens, T. A. Bowden, E. de Wit, F. X. Riedo, V. J. Munster, Case study: Prolonged infectious SARS-CoV-2 shedding from an asymptomatic immunocompromised individual with cancer. *Cell* **183**, 1901–1912.e9 (2020).

23. Z. Luo, L. He, J. Wang, X. Fang, L. Zhang, Developing a combined strategy for monitoring the progress of aptamer selection. *Analyst* **142**, 3136–3139 (2017).

24. K. K. Alam, J. L. Chang, D. H. Burke, FASTAptamer: A bioinformatic toolkit for high-throughput sequence analysis of combinatorial selections. *Mol. Ther. Nucleic Acids* **4**, e230 (2015).

25. M. R. Gotrik, T. A. Feagin, A. T. Csordas, M. A. Nakamoto, H. T. Soh, Advancements in aptamer discovery technologies. *Acc. Chem. Res.* **49**, 1903–1910 (2016).

26. C. Bai, Z. Lu, H. Jiang, Z. Yang, X. Liu, H. Ding, H. Li, J. Dong, A. Huang, T. Fang, Y. Jiang, L. Zhu, X. Lou, S. Li, N. Shao, Aptamer selection and application in multivalent binding-based electrical impedance detection of inactivated H1N1 virus. *Biosens. Bioelectron.* **110**, 162–167 (2018).

27. T. Lu, Q. Ma, W. Yan, Y. Wang, Y. Zhang, L. Zhao, H. Chen, Selection of an aptamer against Muscovy duck parvovirus for highly sensitive rapid visual detection by label-free aptasensor. *Talanta* **176**, 214–220 (2018).

28. B. I. Escudero-Abarca, S. H. Suh, M. D. Moore, H. P. Dwivedi, L. A. Jaykus, Selection, characterization and application of nucleic acid aptamers for the capture and detection of human norovirus strains. *PLOS ONE* **9**, e106805 (2014).

29. T. R. Damase, T. A. Miura, C. E. Parent, P. B. Allen, Application of the open qPCR instrument for the in vitro selection of DNA aptamers against epidermal growth factor receptor and Drosophila C virus. *ACS Comb. Sci.* **20**, 45–54 (2018).

30. J. Hu, J. Kim, C. J. Easley, Quantifying aptamer–protein binding via thermofluorimetric analysis. *Anal. Methods* **7**, 7358–7362 (2015).

31. G. Pérez-Mitta, A. G. Albesa, C. Trautmann, M. E. Toimil-Molares, O. Azzaroni, Bioinspired integrated nanosystems based on solid-state nanopores: "Iontronic" transduction of biological, chemical and physical stimuli. *Chem. Sci.* **8**, 890–913 (2017).

32. U. F. Keyser, Enhancing nanopore sensing with DNA nanotechnology. *Nat. Nanotechnol.* **11**, 106–108 (2016).

33. A. Arima, I. H. Harlisa, T. Yoshida, M. Tsutsui, M. Tanaka, K. Yokota, W. Tonomura, J. Yasuda, M. Taniguchi, T. Washio, M. Okochi, T. Kawai, Identifying single viruses using biorecognition solid-state nanopores. *J. Am. Chem. Soc.* **140**, 16834–16841 (2018).

34. Z. Zhu, D. Wang, Y. Tian, L. Jiang, Ion/molecule transportation in nanopores and nanochannels: From critical principles to diverse functions. *J. Am. Chem. Soc.* **141**, 8658–8669 (2019).

35. Z. Sun, T. Liao, Y. Zhang, J. Shu, H. Zhang, G.-J. Zhang, Biomimetic nanochannels based biosensor for ultrasensitive and label-free detection of nucleic acids. *Biosens. Bioelectron.* **86**, 194–201 (2016).

36. T. Liao, X. Li, Q. Tong, K. Zou, H. Zhang, L. Tang, Z. Sun, G. J. Zhang, Ultrasensitive detection of microRNAs with morpholino-functionalized nanochannel biosensor. *Anal. Chem.* **89**, 5511–5518 (2017).

37. L. Mayne, C.-Y. Lin, S. D. R. Christie, Z. S. Siwy, M. Platt, The design and characterization of multifunctional aptamer nanopore sensors. *ACS Nano* **12**, 4844–4852 (2018).

38. P. Y. Apel, I. V. Blonskaya, S. N. Dmitriev, O. L. Orelovitch, A. Presz, B. A. Sartowska, Fabrication of nanopores in polymer foils with surfactant-controlled longitudinal profiles. *Nanotechnology* **18**, 305302 (2007).

39. G. Pérez-Mitta, A. S. Peinetti, M. L. Cortez, M. E. Toimil-Molares, C. Trautmann, O. Azzaroni, Highly sensitive biosensing with solid-state nanopores displaying enzymatically reconfigurable rectification properties. *Nano Lett.* **18**, 3303–3310 (2018).

40. X. Hou, W. Guo, F. Xia, F.-Q. Nie, H. Dong, Y. Tian, L. Wen, L. Wang, L. Cao, Y. Yang, J. Xue, Y. Song, Y. Wang, D. Liu, L. Jiang, A biomimetic potassium responsive nanochannel: G-quadruplex DNA conformational switching in a synthetic nanopore. *J. Am. Chem. Soc.* **131**, 7800–7805 (2009).

41. Y. Guo, J. Tisoncik, S. McReynolds, M. Farzan, B. S. Prabhakar, T. Gallagher, L. Rong, M. Caffrey, Identification of a new region of SARS-CoV S protein critical for viral entry. *J. Mol. Biol.* **394**, 600–605 (2009).

42. Q. Cui, H. Cheng, R. Xiong, G. Zhang, R. Du, M. Anantpadma, R. Davey, L. Rong, Identification of diaryl-quinoline compounds as entry inhibitors of Ebola virus. *Viruses* **10**, 678 (2018).

43. X. Ou, Y. Liu, X. Lei, P. Li, D. Mi, L. Ren, L. Guo, R. Guo, T. Chen, J. Hu, Z. Xiang, Z. Mu, X. Chen, J. Chen, K. Hu, Q. Jin, J. Wang, Z. Qian, Characterization of spike glycoprotein of SARS-CoV-2 on virus entry and its immune cross-reactivity with SARS-CoV. *Nat. Commun.* **11**, 1620 (2020).

44. J. P. Broughton, W. Deng, C. L. Fasching, J. Singh, Y. Charles, J. S. Chen, M. Biosciences, S. S. Francisco, S. Francisco, S. Francisco, A protocol for rapid detection of SARS-CoV-2 using CRISPR: SARS-CoV-2 DETECTR (Mammoth Biosciences, 2020), pp. 1–9.

45. V. L. Dao Thi, K. Herbst, K. Boerner, M. Meurer, L. P. Kremer, D. Kirrmaier, A. Freistaedter, D. Papagiannidis, C. Galmozzi, M. L. Stanifer, S. Boulant, S. Klein, P. Chlanda, D. Khalid, I. B. Miranda, P. Schnitzler, H.-G. Kräusslich, M. Knop, S. Anders, A colorimetric RT-LAMP assay and LAMP-sequencing for detecting SARS-CoV-2 RNA in clinical samples. *Sci. Transl. Med.* **12**, eabc7075 (2020).

46. P. S. Kwon, S. Ren, S. Kwon, M. E. Kizer, L. Kuo, M. Xie, D. Zhu, F. Zhou, F. Zhang, D. Kim, K. Fraser, L. D. Kramer, N. C. Seeman, J. S. Dordick, R. J. Linhardt, J. Chao, X. Wang, Designer DNA architecture offers precise and multivalent spatial pattern-recognition for viral sensing and inhibition. *Nat. Chem.* **12**, 26–35 (2020).

47. M. Tagliazucchi, O. Azzaroni, I. Szleifer, Responsive polymers end-tethered in solid-state nanochannels: When nanoconfinement really matters. *J. Am. Chem. Soc.* **132**, 12404–12411 (2010).

48. F. M. Gilles, M. Tagliazucchi, O. Azzaroni, I. Szleifer, Ionic conductance of polyelectrolyte-modified nanochannels: Nanoconfinement effects on the coupled protonation equilibria of polyprotic brushes. *J. Phys. Chem. C* **120**, 4789–4798 (2016).

49. Y. Song, J. Song, X. Wei, M. Huang, M. Sun, L. Zhu, B. Lin, H. Shen, Z. Zhu, C. Yang, Discovery of aptamers targeting the receptor-binding domain of the SARS-CoV-2 spike glycoprotein. *Anal. Chem.* **92**, 9895–9900 (2020).

50. A. Schmitz, A. Weber, M. Bayin, S. Breuers, V. Fieberg, M. Famulok, G. Mayer, A SARS-CoV-2 spike binding DNA aptamer that inhibits pseudovirus infection by an RBD-independent mechanism*. *Angew. Chem. Int. Ed.* **60**, 10279–10285 (2021).

51. M. Sun, S. Liu, X. Wei, S. Wan, M. Huang, T. Song, Y. Lu, X. Weng, Z. Lin, H. Chen, Y. Song, C. Yang, Aptamer blocking strategy inhibits SARS-CoV-2 virus infection. *Angew. Chem. Int. Ed.* **60**, 10266–10272 (2021).

52. E. W. Rice, R. B. Baird, A. D. Eaton, Eds., *Standard Methods for the Examination of Water and Wastewater* (American Public Health Association, ed. 23, 2017).

53. J. R. Bolton, K. G. Linden, Standardization of methods for fluence (UV Dose) determination in bench-scale UV experiments. *J. Environ. Eng.* **129**, 209–215 (2003).

54. T. L. Cromeans, X. Lu, D. D. Erdman, C. D. Humphrey, V. R. Hill, Development of plaque assays for adenoviruses 40 and 41. *J. Virol. Methods* **151**, 140–145 (2008).

55. A. M. Gall, J. L. Shisler, B. J. Mariñas, Inactivation kinetics and replication cycle inhibition of adenovirus by monochloramine. *Environ. Sci. Technol. Lett.* **49**, 4584–4590 (2016).

56. L. Zhang, X. Fang, X. Liu, H. Ou, H. Zhang, J. Wang, Q. Li, H. Cheng, W. Zhang, Z. Luo, Discovery of sandwich type COVID-19 nucleocapsid protein DNA aptamers. *Chem. Commun.* **56**, 10235–10238 (2020).